SUPPLEMENTARY ONLINE MATERIAL

All of the many-body phenomena (local field effects, excitation-induced dephasing and frequency shift and biexciton formation) contribute to the observed SIII signal. For co-circular excitation, mixed biexciton formation should dominate. However we observe an additional signal that oscillates at twice the HH exciton emission frequency during the 2QC time. Here, we show by a perturbative solution of the modified optical Bloch equations (MOBE) for a two-level system that this signal results from interaction-induced effects other than biexciton formation. The MOBE are derived from the optical Bloch equations for a two-level system by including phenomenological exciton interaction terms. These modify the dephasing rate and transition frequency proportional to the population of excitons in the system, and the driving field proportional to the exciton polarization.

$$\begin{aligned} &\dot{p} + (\gamma + \gamma' Nn)p + i(\Omega + \Omega' Nn)p + \tfrac{i}{\hbar}[\mu(E(R,t) + Lp)][1 - 2n] = 0 \\ &\dot{n} + \gamma_r n + \tfrac{i}{\hbar}[\mu(E(R,t) + Lp)][p^* - p] = 0 \end{aligned} \qquad (1)$$

Here, n and p are the diagonal and off-diagonal terms of the two-level density matrix. The optical Bloch equation terms are the transition frequency Ω, homogenous dephasing rate γ, recombination rate γ_r, transition dipole moment μ, and electric field $E(R,t)$. The phenomenological interaction-induced terms are the excitation-induced frequency shift Ω' and dephasing rate γ', which are proportional to the initial ground state population N, and the contribution of local fields L. Next, we expand the MOBE perturbatively in the density matrix elements and the electric field.

$$\begin{aligned} &\dot{p}^{(1)} + \gamma p^{(1)} + i\Omega p^{(1)} + \tfrac{i}{\hbar}\mu E(R,t) = 0 \\ &\dot{n}^{(2)} + \gamma_r n^{(2)} + \tfrac{i}{\hbar}\mu[E(R,t)p^{*(1)} - E^*(R,t)p^{(1)}] = 0 \\ &\dot{p}^{(3)} + \gamma p^{(3)} + i\Omega p^{(3)} - \tfrac{i}{\hbar}\mu[2E(R,t) + \Lambda p^{(1)}]n^{(2)} = 0 \end{aligned} \qquad (2)$$

Only the third order signal depends on the interaction-induced terms, Λ, and we approximate the electric field as a series of three delta function pulses with different wavevectors.

$$\Lambda = 2L + {}^{i\hbar}\!/_{\mu} N(\gamma' + i\Omega')$$
$$E(R,t) = \varepsilon_A \delta(t - t_A) e^{ik_A R - i\omega t} + \varepsilon_B \delta(t - t_B) e^{ik_B R - i\omega t} + \varepsilon_C \delta(t - t_C) e^{ik_C R - i\omega t} \qquad (3)$$

We solve this set of coupled differential equations to obtain the third order polarization and only retain the terms which satisfy the phase matching condition, $k_{sig} = k_A + k_B - k_C$. For this time-ordering the OBE terms cancel for a two level system and only the interaction-induced terms contribute, so that

$$p^{(3)}_{ABC*}(\tau_2, \tau_3) = \mathbf{4}\Lambda({}^{\mu}\!/_{\hbar})^3 \varepsilon_A \varepsilon_B \varepsilon_C e^{-i\omega(\tau_2 + \tau_3)} \Theta(\tau_2)\Theta(\tau_3) \exp[-\mathbf{2}(\gamma + i\Omega)\tau_2 - (\gamma + i\Omega)\tau_3] \qquad (4)$$

where $\tau_2 = t_C - t_B$ and $\tau_3 = t - t_C$, $\Theta(\tau)$ is the Heaviside step function and we assume long recombination times. The first term in the exponent gives the time dependence of the signal during τ_2, the two-quantum coherence time. Therefore, the interaction-induced phenomena lead to a doubled oscillation frequency and dephasing rate which we observe during the 2QC time in our measurements using co-circularly polarized excitation. Note that the dephasing rate and frequency shift are not affected by the excited carrier density, which is in contradiction to our measurements. In other words, the perturbative solution gives the origin of the signal but not its detailed behavior, as discussed previously by Shacklette and Cundiff (Ref #14). The treatment can be improved by solving the set of coupled differential equations given by the MOBE using a numerical technique which selects the relative signal based on a spatial Fourier expansion of the density matrix.

In Fig. S1 we show the deconvolved two-quantum coherence transients for the HH-HH (A) and mixed (B) HH-LH biexcitons and the HH exciton interaction-induced effect (C). The polarization and spectral selectivity and the phase sensitivity of this experiment allow us to obtain and separate the full signal fields produced by these many-

body phenomena. For comparison, we collected a spectrally resolved time-integrated four-wave mixing signal for co-circular excitation, shown in Fig. S2.

Next we demonstrate how rotating frame detection affects the peak positions of the biexciton coherence features in our SIII measurements. Rotating frame detection in our experiment is afforded by the use of an SLM to impart envelope delays to the excitation pulses without shifting the carrier phase. Therefore, the coherences that evolved during τ_2 were resolved by interferometric detection and referenced to the user-defined carrier frequency, ω_0. Figs. S3 A and B show surfaces from two SIII measurements using linearly polarized excitation with two different carrier frequencies 363.4 THz and 353.5 THz, respectively. It is clear that the main features, resulting from biexciton coherences, shift by twice the change in the carrier frequency. We also made SI measurements using different carrier frequencies. Here the features depend on single exciton coherences and were shifted by the change in the carrier frequency rather than twice that amount.

Finally we discuss the present 2Q-2D FTS measurements in relation to 1D four-wave mixing experiments at negative probe delay times. In the latter experiments, the sample is interrogated by two ultrafast pulses that propagate in two separate beams with wavevectors k_1 and k_2. The signal is the "self-diffraction" of the k_2 pulse during the emission time, t, into the phase-matched direction $2k_2 - k_1$ and is detected as a function of the delay between the two pulses, τ. The k_2 field interacts twice with the sample, at positive delay times playing the role of both pump (along with the k_1 field, generating sample responses at the difference wavevector $k_2 - k_1$) and probe. The signal emission can be detected in a number of ways, for instance integrated over t, frequency-resolved in the emission frequency, or time-resolved through the use of a separate gating pulse. However, unlike 2DFTS, none of these methods is phase-sensitive to the coherences during τ or can relate them to the signal emission frequencies. When the k_2 pulse precedes the k_1 pulse, typically designated as $\tau < 0$, the two interactions of the k_2 field create various two-exciton coherences (like those that contribute to signals in Figs. 3 B and C) that have different frequencies and dephasing rates. The k_1 pulse then probes the system

by converting the two-exciton coherences to one-exciton coherences that radiate during *t*. Even if the emission is frequency-resolved, multiple contributions at common emission frequencies but at different 2QC frequencies that are neatly separated along the vertical axis in the 2D measurement (Figs. 3 B and C) are highly convolved in the 1D case. Our 2Q-2D FTS measurements are phase-sensitive to the two-exciton coherences, thereby providing a second frequency axis along which these two-quantum coherences can be spread out. Also, all of the ultrafast optical pulses are interferometrically stable, allowing the two-quantum coherences that evolve during τ to be mapped to distinct one-quantum coherences that evolve during *t*, therefore revealing how the many-particle states are coupled to each other.

FIGURE CAPTIONS

Fig. S1. The 2QC transients were extracted from the 2D FTS data by selecting the HH emission frequency from the cross-circular excitation experiment to obtain the (A) HH biexciton transient, or from the co-circular experiment to obtain the (C) HH exciton interaction transient; or selecting the LH emission frequency from the co-circular experiment to obtain (B) the mixed biexciton transient. It is clear that the phase sensitivity and spectral selectivity of the 2Q 2D FTS measurement allows the contribution of synchronous many-body phenomena to be separated.

Fig. S2. Results from a traditional 1D spectrally-resolved four-wave mixing measurement done with co-circular, time-coincident pump beams E_A and E_B and probe E_C (no LO field). The modulations of signals at the two prominent emission frequencies arise from multiple interfering contributions to those signals. The contributions are separated in the 2D measurement with co-circular pump beams (Fig. 3C).

Fig. S3. SIII surfaces generated using linearly polarized excitation pulses in which the carrier frequency, ω_0, was changed from (A) 363.4 THz to (B) 353.5 THz. The prominent HH biexciton feature remains at the same emission frequency, ω, but is shifted along ω_2 depending on the carrier frequency selected. In A (B), where the carrier frequency is 9 THz (19 THz) lower than the HH resonance, the biexciton feature appears at approximately 18 THz (38 THz) along the ω_2 axis. The blue line plotted at $\omega_2 = 2(\omega - \omega_0)$ is shown for reference.

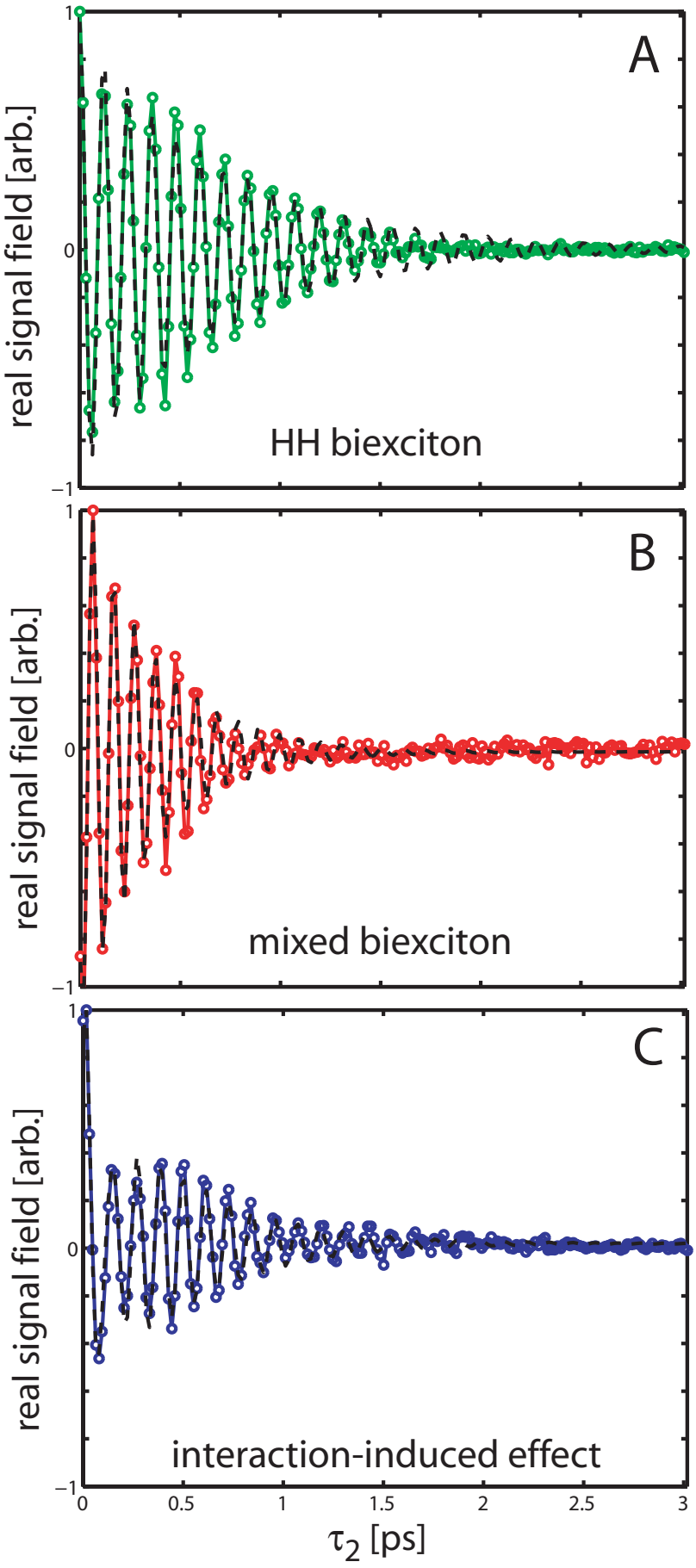
A
real signal field [arb.]
HH biexciton
B
real signal field [arb.]
mixed biexciton
C
real signal field [arb.]
interaction-induced effect
1
0
−1
0
0.5
1
1.5
2
2.5
3
τ2 [ps]

Fig. S1.

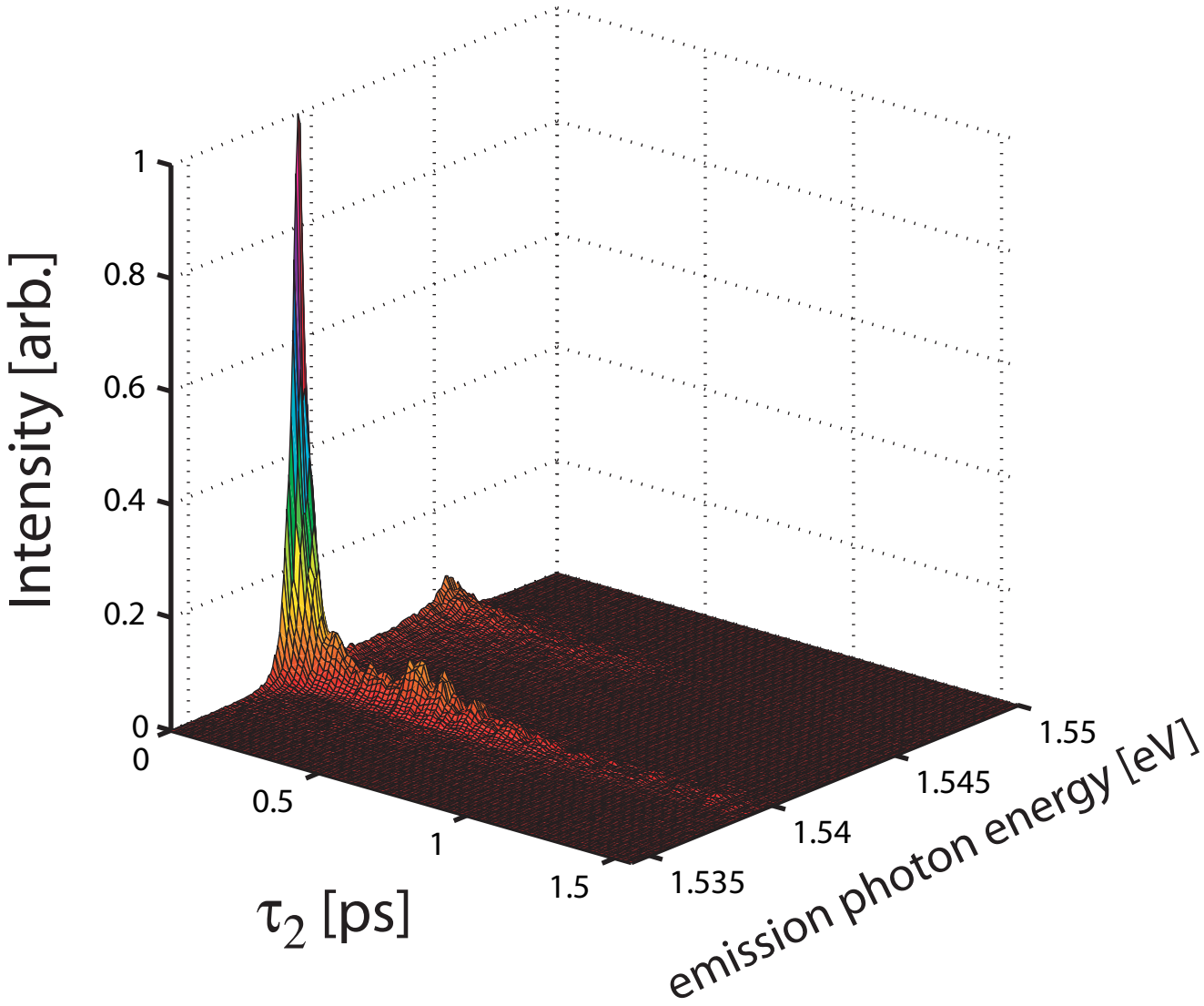
Intensity [arb.]
1
0.8
0.6
0.4
0.2
0
0
0.5
1
1.5
τ2 [ps]
1.535
1.54
1.545
1.55
emission photon energy [eV]

Fig. S2.

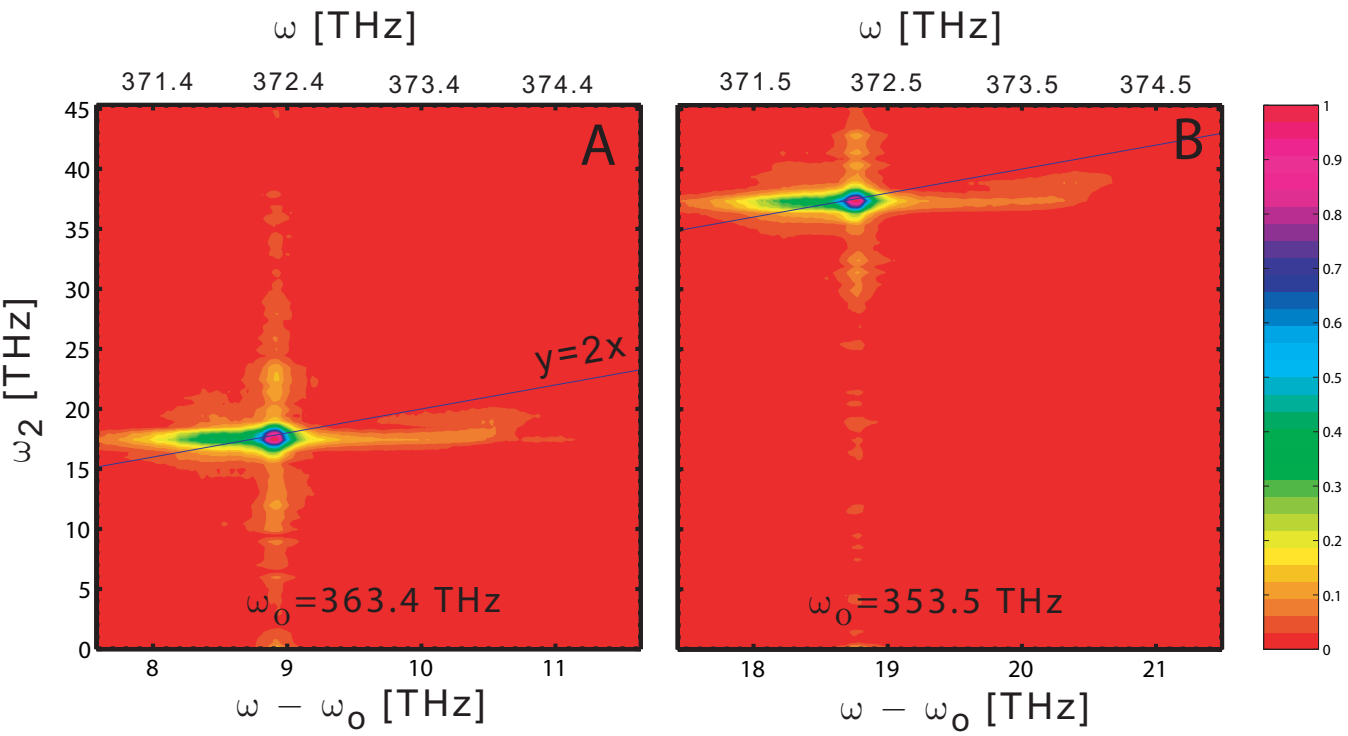
ω [THz]
371.4
372.4
373.4
374.4
A
y=2x
ω2 [THz]
ω0=363.4 THz
ω − ω0 [THz]
ω [THz]
371.5
372.5
373.5
374.5
B
ω0=353.5 THz
ω − ω0 [THz]

Fig. S3.